Optics Communications 282 (2009) 1516–1520

Contents lists available at ScienceDirect

Optics Communications

journal homepage: www.elsevier.com/locate/optcom

Dual-frequency paired polarization phase shifting ellipsometer

Chih-Jen Yu [a], Chu-En Lin [a], Hui-Kang Teng [b], Chien-Chung Tsai [c], Chien Chou [a,d,e,*]

[a] Department of Optics and Photonics, National Central University, Jhongli 320, Taiwan
[b] Graduate Institute of Electrical Engineering, Nan-Kai Institute of Technology, NanTou 542, Taiwan
[c] Graduate Institute of Photonics and Optoelectronics, Department of Electrical Engineering, National Taiwan University, Taipei 106, Taiwan
[d] Department of Biomedical Imaging and Radiological Science, Institute of Biophotonics, National Yang-Ming University, 155 Li-Nong St. Sec. 2, Pei-Tou, Taipei 112, Taiwan
[e] Graduate Institute of Electro-Optical Engineering, Chang Gung University, Taoyuan 333, Taiwan

ARTICLE INFO

Article history:
Received 25 September 2008
Received in revised form 27 December 2008
Accepted 5 January 2009

Keywords:
Optical heterodyne interferometer
Ellipsometry
Dual-frequency laser
Phase shifting technique

ABSTRACT

A novel dual-frequency paired polarization phase shifting ellipsometer (DPPSE) is proposed and experimentally demonstrated. It combines the features of the phase shifting interferometer and common-path polarized heterodyne interferometric ellipsometer where the ellipsometric parameters (EP) of a specimen are measured accurately. The experimental results verify that DPPSE is capable of determining the full dynamic range of EP. In addition, the properties of dual-frequency paired linearly polarized laser beam in DPPSE perform in common phase noise rejection mode. It is insensitive to environmental disturbance and laser frequency noise. The capability of DPPSE to perform higher accuracy EP measurement than conventional ellipsometer is verified according to error analysis.

1. Introduction

Ellipsometry is a well-developed method that is able to accurately characterize the optical properties of specimen by measuring the ellipsometric parameters (EP) versus the emerging laser beam reflected by the specimen [1–3]. Among different kinds of optical ellipsometers, the photometric ellipsometer (PE) uses laser intensity modulation technique that can measure EP precisely by measuring the amplitude attenuation and phase shift of the emerging laser beam in real time [1,2]. There are different methods to modulate a laser beam, such as by rotating the analyzer in rotating analyzer ellipsometer (RAE) [4–7], or by using photo-elastic modulator (PEM) in polarization modulation ellipsometer (PME) [8,9]. However, higher laser intensity noise in RAE or PME reduces the signal-to-noise ratio (SNR) on detected signal [2,10]. Meanwhile, the limited rotation speed and mechanical instability of the intensity modulation in RAE or the existing residual birefringence in PEM on phase modulation in PME apparently causes less sensitivity in EP measurements [8,11]. Aspnes [6] has calculated the measurement uncertainty by RAE. The result shows that the uncertainty in one of the EP(Δ), which is the phase retardation between linearly polarized p and s waves, becomes large when Δ is close to 0° or 180° (i.e., $|\cos\Delta| \approx 1$). In addition, RAE and PME, both based on intensity measurement, introduce an ambiguity on Δ that results in a limited dynamic range of $0° < \Delta < 180°$ [1,2]. To avoid these disadvantages on Δ measurement, a rotating compensator is introduced in RAE which then becomes the rotating compensator ellipsometer (RCE), and is able to measure EP properly by using Fourier transform analysis [12].

Recently, Chou et al. [13] proposed a polarization modulation imaging ellipsometer (PMIE) by rotating a quarter wave plate at five specific azimuthal angles sequentially. Five corresponding images are recorded by using a CCD camera. Thus, two-dimensional (2-D) distributions of EP are available at the same time. In addition, the rotating quarter wave plate located after a specimen in PMIE can achieve full dynamic range of EP measurement and is insensitive to the laser intensity fluctuation. Han and Chiao [14] also proposed a stroboscopic illumination technique for 2-D distribution of EP measurements. However, it results in limited dynamic range on ψ, another EP which is the arctangent of the ratio of the reflectivity of p and s waves. In order to increase the sensitivity on EP measurement, a polarized heterodyne interferometric ellipsometer is proposed that is able to accurately characterize the EP of specimen [15–17]. However, the speed of phase measurement was limited by the use of a lock-in amplifier. In this research, we propose an optical heterodyne ellipsometer that integrates common-path heterodyne and phase shifting interferometer with a dual-frequency paired linear polarizations [18]. Thus, the dual-frequency paired

* Corresponding author. Address: Department of Biomedical Imaging and Radiological Science, Institute of Biophotonics, National Yang-Ming University, 155 Li-Nong St. Sec. 2, Pei-Tou, Taipei 112, Taiwan. Tel.: +886 2 28267061; fax: +886 2 28201095.
E-mail address: cchou@ym.edu.tw (C. Chou).

0030-4018/$ - see front matter © 2009 Elsevier B.V. All rights reserved.
doi:10.1016/j.optcom.2009.01.001

polarizations phase shifting ellipsometer (DPPSE) is proposed and set up. The phase shifting technique integrated into DPPSE fully expands the dynamic range of EP. This overcomes the limitation of conventional ellipsometer based on intensity modulation in measurement [1,2]. In this paper, the working principle of DPPSE is described in Section 2, while the experimental setup and results are shown in Section 3. In addition, the error in EP measurement is analyzed and computer simulated in Section 4. The conclusions and discussion are given in the last section.

2. Working principle of DPPSE

A dual-frequency linearly polarized laser beam is produced by using a frequency stabilized linearly polarized He–Ne laser beam integrated with an electro-optic modulator (EOM) that is driven at frequency ω [19]. Thus, a pair of highly correlated orthogonal linearly polarized light waves (p and s waves), which slightly differ on temporal frequency ($\omega_p = \omega_0 + (\omega/2)$ and $\omega_s = \omega_0 - (\omega/2)$), is generated. The p-polarized wave is along the *x*-axis, and the s-polarized wave is along the *y-axis*. Thus, the Jones vector is expressed by

$$\mathbf{E_0} = \begin{pmatrix} \exp(i\omega t/2) \\ \exp(-i\omega t/2) \end{pmatrix} a_0 \exp(i\omega_0 t), \tag{1}$$

where a_0 is the output amplitude and ω_0 is the central frequency of laser beam. The laser beam passes through a polarizer whose transmission axis is set up at 45° to the *x-axis*. The Jones vector of the emerging beam is then expressed as

$$\begin{aligned} \mathbf{E_{DL}} &= \frac{1}{2}\begin{pmatrix} 1 & 1 \\ 1 & 1 \end{pmatrix}\begin{pmatrix} \exp(i\omega t/2) \\ \exp(-i\omega t/2) \end{pmatrix} a_0 \exp(i\omega_0 t) \\ &= \begin{pmatrix} 1 \\ 1 \end{pmatrix} a_0 \cos\frac{\omega t}{2} \exp(i\omega_0 t). \end{aligned} \tag{2}$$

Therefore, p and s waves in Eq. (2) are with equal amplitude and zero phase difference. This generates a dual-frequency paired linearly polarized laser beam, which can be expressed by Stokes vector $\mathbf{S_{DL}}$ as

$$\mathbf{S_{DL}} = (1 \quad 0 \quad 1 \quad 0)^{\mathrm{T}} I_0(1 + \cos\omega t), \tag{3}$$

where $I_0 = a_0^2$ is defined and the superscript T means transpose. Meanwhile, the general representation of the Mueller matrix $\mathbf{M_S}$ of the specimen [1] is

$$\mathbf{M_S} = R\begin{pmatrix} 1 & -\cos 2\psi & 0 & 0 \\ -\cos 2\psi & 1 & 0 & 0 \\ 0 & 0 & \sin 2\psi\cos\Delta & \sin 2\psi\sin\Delta \\ 0 & 0 & -\sin 2\psi\sin\Delta & \sin 2\psi\cos\Delta \end{pmatrix}, \tag{4}$$

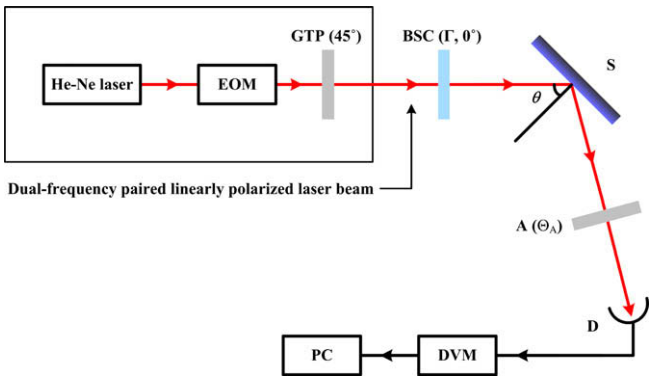

Fig. 1. The setup of DPPSE. EOM: electro-optic modulator, GTP: Glan–Thompson polarizer, BSC: Babinet–Soleil compensator, S: specimen, A: analyzer, D: photo detector, DVM: digital voltmeter, PC: personal computer.

where R is the reflectance and the EP, ψ and Δ, are defined by

$$\psi = \tan^{-1}(|r_p|/|r_s|), \tag{5a}$$

$$\Delta = \varphi_p - \varphi_s. \tag{5b}$$

where (r_p, r_s) and (φ_p, φ_s) are the amplitude reflection coefficients and phase shift of p- and s-polarized waves by specimen, respectively. In Fig. 1, dual-frequency paired linearly polarized laser beam is normal incident on Babinet–Soleil compensator (BSC), and then impinges onto a specimen and an analyzer (A) of its azimuthal angle at Θ_A to *x-axis*. The Mueller matrices of BSC and analyzer are expressed as

$$\mathbf{M_{BSC}} = T_{BSC}\begin{pmatrix} 1 & 0 & 0 & 0 \\ 0 & 1 & 0 & 0 \\ 0 & 0 & \cos\Gamma & \sin\Gamma \\ 0 & 0 & -\sin\Gamma & \cos\Gamma \end{pmatrix}, \tag{6a}$$

$$\mathbf{M_A} = T_A\begin{pmatrix} 1 & \cos 2\Theta_A & \sin 2\Theta_A & 0 \\ \cos 2\Theta_A & \cos^2 2\Theta_A & \sin 2\Theta_A\cos 2\Theta_A & 0 \\ \sin 2\Theta_A & \sin 2\Theta_A\cos 2\Theta_A & \sin^2 2\Theta_A & 0 \\ 0 & 0 & 0 & 0 \end{pmatrix}. \tag{6b}$$

Also, the Stokes vector of a photo detector **D** is expressed as

$$\mathbf{D} = k(1 \quad 0 \quad 0 \quad 0), \tag{6c}$$

T_{BSC} and T_A are the transmittance of BSC and analyzer, respectively; Γ is the phase retardation of BSC; and k means the quantum efficiency of photo detector. Hence, the intensity of the emerging beam can be described by

$$\mathbf{S_{out}} = \mathbf{M_A M_S M_{BSC} S_{DL}}, \tag{7a}$$

$$I = \mathbf{D}\mathbf{S_{out}} = \tilde{I} + \tilde{I}\cos\omega t, \tag{7b}$$

$$\tilde{I} = TI_0[1 - \cos 2\psi\cos 2\Theta_A + \sin 2\psi\cos(\Delta + \Gamma)\sin 2\Theta_A], \tag{7c}$$

$$T = kT_A T_{BSC} R, \tag{7d}$$

According to Eq. (7b), both dc and ac terms are with equal amplitude. Thus, $\tilde{I}$ can be obtained either by ac or dc component, whereas ac is preferred in this experiment. If Γ of BSC is adjusted at 0° and Θ_A is set either at 0° or 90° then, from Eq. (7c),

$$\tilde{I}_p = 2TI_0\sin^2\psi, \quad \text{at } \Theta_A = 0°, \tag{8a}$$

$$\tilde{I}_s = 2TI_0\cos^2\psi, \quad \text{at } \Theta_A = 90°, \tag{8b}$$

and

$$\psi = \tan^{-1}\left(\tilde{I}_p/\tilde{I}_s\right)^{1/2}. \tag{9}$$

Similarly, when the analyzer is set at 45° to the *x-axis*, then

$$\tilde{I}_{45°} = T_0 I_0[1 + \sin 2\psi\cos(\Delta + \Gamma)], \tag{10}$$

Thus, Δ can be obtained by shifting the phase retardation Γ of BSC at 0°, 90°, 180°, and 270° sequentially.

$$\tilde{I}_1 = T_0 I_0(1 + \sin 2\psi\cos\Delta), \quad \text{at } \Gamma = 0°, \tag{11a}$$

$$\tilde{I}_2 = T_0 I_0(1 - \sin 2\psi\sin\Delta), \quad \text{at } \Gamma = 90°, \tag{11b}$$

$$\tilde{I}_3 = T_0 I_0(1 - \sin 2\psi\cos\Delta), \quad \text{at } \Gamma = 180°, \tag{11c}$$

$$\tilde{I}_4 = T_0 I_0(1 + \sin 2\psi\sin\Delta), \quad \text{at } \Gamma = 270°. \tag{11d}$$

We define

$$\alpha = \frac{\tilde{I}_1 - \tilde{I}_3}{\tilde{I}_1 + \tilde{I}_3} = \sin 2\psi\cos\Delta, \tag{12a}$$

$$\beta = \frac{\tilde{I}_4 - \tilde{I}_2}{\tilde{I}_4 + \tilde{I}_2} = \sin 2\psi\sin\Delta, \tag{12b}$$

Table 1
Determination of Δ in full range from 0° to 360°, where $\alpha = \sin 2\psi \cos\Delta$ and $\beta = \sin 2\psi \sin\Delta$.

α and β	Δ
$\alpha \geqslant 0$ and $\beta \geqslant 0$	$0° \leqslant \Delta \leqslant 90°$
$\alpha \leqslant 0$ and $\beta \geqslant 0$	$90° \leqslant \Delta \leqslant 180°$
$\alpha \leqslant 0$ and $\beta \leqslant 0$	$180° \leqslant \Delta \leqslant 270°$
$\alpha \geqslant 0$ and $\beta \leqslant 0$	$270° \leqslant \Delta \leqslant 360°$

then Δ is calculated by

$$\Delta = \tan^{-1}(\beta/\alpha). \tag{13}$$

From Eqs. (9) and (13), ψ and Δ are independent of I_0 and the laser intensity fluctuation is independent of the measurements. According to Eq. (9), the dynamic range of ψ is $0° < \psi < 90°$. It can also be extended to a full dynamic range of $0° < \Delta < 360°$ under the condition shown in Table 1.

3. Experimental setup and results

3.1. Experimental details

The optical setup of DPPSE is shown in Fig. 1 in which a dual-frequency laser beam is generated by using a linearly polarized He–Ne laser (Spectral physics, 117A) at 632.8 nm in conjunction with an EOM (New focus, 4002) whose driving frequency is operated at 2 kHz. Two Glan–Thompson polarizers are used: one is used as a polarizer and the other is used as an analyzer in this setup. Before the specimen is placed in the optical setup, the azimuthal angles of the polarizer and analyzer are set at 0° and 90°, respectively, in order to calibrate the BSC (Special Optics, 8-400-UNCTD) in accordance with the standard calibration procedure provided by the manufacturer [20]. The displacement of generating 360° phase shift in BSC is 13.355 mm by using 632.8 nm of the wavelength. The phase retardation of BSC on 0°, 90°, 180°, and 270° are then calibrated using a digital micrometer in the BSC at 0 mm, 3.339 mm, 6.678 mm, and 10.016 mm on displacement, respectively, whereas, the resolution of digital micrometer is 0.001 mm. Meanwhile, a digital voltmeter (Agilent 34401A) is used to measure the intensity of signal. The measured time which includes 4 steps of phase shifting and data acquisition times is 4 min.

3.2. Measurement of the complex refractive index of a bare silicon wafer

In order to demonstrate the capability of DPPSE able to measure the EP of a low absorbed material ($k \simeq 0$) of which the phase retardation Δ is close to 0° or 180° for various incident angles [1], a bare silicon wafer was tested for the verification. The incident angle θ was set at 80°. The complex refraction index N ($N = n - ik$) of a bared silicon wafer is calculated in Table 2. This shows the ability of DPPSE to accurately measure Δ of low k material in comparison with the conventional RAE [6] experimentally.

Table 2
Measured data of a bared silicon wafer at incident angle $\theta = 80°$[a].

	Ellipsometric parameters		Refractive index	
	ψ (°)	Δ (°)	n	k
Measured	10.62	0.59	3.95	0.015
Calculated	11.16	0.73	3.88	0.019

[a] The calculated EP (ψ, Δ) is computed by using Matlab 7.0.1 program.

3.3. Measurement of the thickness of a thin SiO_2 film

A step wafer was also tested in order to demonstrate the capability of DPPSE to measure thin film thickness. The calibrated step wafer (Mikropack ID0153) in which the silicon dioxide thin film was deposited on the silicon substrate [21] was tested. Table 3 shows the results at different areas that present different thickness. The incident angle of laser beam was 70° in this experiment. The well agreement between measured and calibrated data clearly demonstrates the accuracy of DPPSE.

4. Error analysis

Because the extinction ratio of the Glan–Thompson polarizer or analyzer is 10^5, the elliptical polarization of an incident beam can be reduced significantly. However, the improper phase retardation of BSC and the misalignment of the polarizer and analyzer introduce uncertainties in the EP measurement. According to the error propagation method [22], the total uncertainty can be expressed as the sum of the square of each error source

$$\delta\psi_t = [(\delta\psi_P)^2 + (\delta\psi_\Gamma)^2 + (\delta\psi_A)^2]^{1/2}, \tag{14a}$$
$$\delta\Delta_t = [(\delta\Delta_P)^2 + (\delta\Delta_\Gamma)^2 + (\delta\Delta_A)^2]^{1/2}, \tag{14b}$$

where $\delta\psi$ and $\delta\Delta$ are measured uncertainties of ψ and Δ, respectively. The subscripts P and A denote the misalignment of the polarizer and analyzer, respectively, and the subscript Γ means the error of the phase retardation of BSC. Meanwhile, the subscript t denotes a summation of each error source.

To calculate $\delta\psi_P$ and $\delta\Delta_P$ of the uncertainty induced by polarizer misalignment, the detected intensity I needs to be recalculated by assuming that the azimuthal angle of polarizer is at Θ_P, which does not equal to 45° in this calculation. Then Eq. (7b) becomes

$$\begin{aligned} I &= \mathbf{D}\mathbf{M_A}\mathbf{M_S}\mathbf{M_{BSC}}\mathbf{M_P}\mathbf{S_0} \\ &= TI_0\{(1 - \cos 2\psi \cos 2\Theta_P) + (\cos 2\Theta_P - \cos 2\psi)\cos 2\Theta_A \\ &\quad + [\sin 2\Theta_P \sin 2\psi \cos(\Delta + \Gamma)] \sin 2\Theta_A\}(1 + \sin 2\Theta_P \cos\omega t) \\ &= \bar{I} + \tilde{I}\cos\omega t, \end{aligned} \tag{15a}$$

and

$$\mathbf{S_0} = (1 \quad 0 \quad \cos\omega t \quad -\sin\omega t)^T, \tag{15b}$$
$$\begin{aligned} \bar{I} &= TI_0\{(1 - \cos 2\psi \cos 2\Theta_P) + (\cos 2\Theta_P - \cos 2\psi)\cos 2\Theta_A \\ &\quad + [\sin 2\Theta_P \sin 2\psi \cos(\Delta + \Gamma)] \sin 2\Theta_A\}, \end{aligned} \tag{15c}$$
$$\tilde{I} = \bar{I} \sin 2\Theta_P. \tag{15d}$$

$\mathbf{M_P}$ is the Mueller matrix of the misaligned polarizer, $\bar{I}$ and $\tilde{I}$ are dc and ac components of the measured intensity, respectively. Because the ac term of $\tilde{I}$ is our interest, the measured intensities when the analyzer are rotated at 0°, 90° are

$$\tilde{I}_p = 2TI_0 \sin^2\psi(1 + \cos 2\Theta_P)\sin 2\Theta_P, \quad \text{at } \Theta_A = 0°, \tag{16a}$$
$$\tilde{I}_s = 2TI_0 \cos^2\psi(1 - \cos 2\Theta_P)\sin 2\Theta_P, \quad \text{at } \Theta_A = 90°. \tag{16b}$$

Table 3
The measurement of thickness of SiO_2 thin film deposited on a silicon substrate at incident angle $\theta = 70°$[a].

Area	Ellipsometric parameters		Thickness
	ψ (°)	Δ (°)	T (nm)
#3: Measured	11.14	162.42	290.95
#3: Calibrated	10.83	162.23	290.16
#4: Measured	38.93	280.26	187.96
#4: Calibrated	38.30	280.06	189.20

[a] The calibrated data is from Ref. [20].

Similarly, when $\Theta_A = 45^\circ$

$$\tilde{I}_{45^\circ} = TI_0[1 - \cos 2\psi \cos 2\Theta_P + \sin 2\Theta_P \sin 2\psi \cos(\Delta + \Gamma)] \sin 2\Theta_P, \tag{17a}$$

then

$$\tilde{I}_1 = TI_0(1 - \cos 2\psi \cos 2\Theta_P + \sin 2\Theta_P \sin 2\psi \cos\Delta) \sin 2\Theta_P, \text{ at } \Gamma = 0^\circ, \tag{17b}$$

$$\tilde{I}_2 = TI_0(1 - \cos 2\psi \cos 2\Theta_P - \sin 2\Theta_P \sin 2\psi \sin\Delta) \sin 2\Theta_P \text{ at } \Gamma = 90^\circ, \tag{17c}$$

$$\tilde{I}_3 = TI_0(1 - \cos 2\psi \cos 2\Theta_P - \sin 2\Theta_P \sin 2\psi \cos\Delta) \sin 2\Theta_P, \text{ at } \Gamma = 180^\circ, \tag{17d}$$

and

$$\tilde{I}_4 = TI_0(1 - \cos 2\psi \cos 2\Theta_P + \sin 2\Theta_P \sin 2\psi \sin\Delta) \sin 2\Theta_P, \text{ at } \Gamma = 270^\circ. \tag{17e}$$

Theoretically, the uncertainties of $\delta\psi_P$ and $\delta\Delta_P$ can be obtained by

$$(\delta\psi_P)^2 = \left(\frac{\partial\psi}{\partial\tilde{I}_p}\right)^2 \left(\frac{\partial\tilde{I}_p}{\partial\Theta_P}\right)^2 (\delta\Theta_P)^2 + \left(\frac{\partial\psi}{\partial\tilde{I}_s}\right)^2 \left(\frac{\partial\tilde{I}_s}{\partial\Theta_P}\right)^2 (\delta\Theta_P)^2, \tag{18a}$$

$$(\delta\Delta_P)^2 = \sum_{i=1}^{4} \left(\frac{\partial\Delta}{\partial\tilde{I}_i}\right)^2 \left(\frac{\partial\tilde{I}_i}{\partial\Theta_P}\right)^2 (\delta\Theta_P)^2, \tag{18b}$$

where $\delta\Theta_P$ denotes the misaligned angle of the polarizer. By substituting Eqs. (9) and (16) into Eq. (18a), the calculated result $\delta\psi_P$ becomes

$$(\delta\psi_P)^2 = \frac{1}{2}\sin^2 2\psi (\delta\Theta_P)^2, \tag{19a}$$

By substituting Eqs. (13) and (17) into Eq. (18b), the uncertainty $\delta\Delta_P$ becomes

$$(\delta\Delta_P)^2 = (2\cot^2 2\psi + \cos^2 2\psi \sin^2 2\Delta)(\delta\Theta_P)^2. \tag{19b}$$

Similarly, the uncertainty of EP that is induced by the error of phase retardation of BSC can be described as

$$(\delta\psi_\Gamma)^2 = \left(\frac{\partial\psi}{\partial\tilde{I}_p}\right)^2 \left(\frac{\partial\tilde{I}_p}{\partial\Gamma}\right)^2 (\delta\Gamma)^2 + \left(\frac{\partial\psi}{\partial\tilde{I}_s}\right)^2 \left(\frac{\partial\tilde{I}_s}{\partial\Gamma}\right)^2 (\delta\Gamma)^2, \tag{20a}$$

$$(\delta\Delta_\Gamma)^2 = \sum_{i=1}^{4} \left(\frac{\partial\Delta}{\partial\tilde{I}_i}\right)^2 \left(\frac{\partial\tilde{I}_i}{\partial\Gamma}\right)^2 (\delta\Gamma)^2, \tag{20b}$$

where $\delta\Gamma$ is the variance of phase retardation of BSC. By substituting Eqs.(8)–(13) into Eqs. (20a) and (20b), the uncertainty $\delta\psi_\Gamma$ and $\delta\Delta_\Gamma$ are calculated as

$$(\delta\psi_\Gamma)^2 = 0, \tag{21a}$$

$$(\delta\Delta_\Gamma)^2 = \frac{1}{2}(\sin^4\Delta + \cos^4\Delta + \frac{1}{4}\sin^2 2\psi \sin^2 2\Delta)(\delta\Gamma)^2. \tag{21b}$$

According to the result of Eq. (21a), ψ is insensitive to phase retardation error of BSC, while Δ is dependent on it. Inasmuch as the resolution of BSC is 0.001 mm, this indicates the deviation of BSC at $\delta\Gamma \simeq 0.003^\circ$. The computer simulation of $\delta\Delta_\Gamma$ is shown in Fig. 2, which is a periodic function of ψ and Δ. The uncertainty $\delta\Delta_\Gamma$ is in the range of $0.015^\circ < \delta\Delta_\Gamma < 0.021^\circ$ for all ψ and Δ. Also, the uncertainties from misalignment of the analyzer are expressed by

$$(\delta\psi_A)^2 = \left(\frac{\partial\psi}{\partial I_p}\right)^2 \left(\frac{\partial I_p}{\partial\Theta_A}\right)^2 (\delta\Theta_A)^2 + \left(\frac{\partial\psi}{\partial I_s}\right)^2 \left(\frac{\partial I_s}{\partial\Theta_A}\right)^2 (\delta\Theta_A)^2, \tag{22a}$$

$$(\delta\Delta_A)^2 = \sum_{i=1}^{4} \left(\frac{\partial\Delta}{\partial\tilde{I}_i}\right)^2 \left(\frac{\partial\tilde{I}_i}{\partial\Theta_A}\right)^2 (\delta\Theta_A)^2, \tag{22b}$$

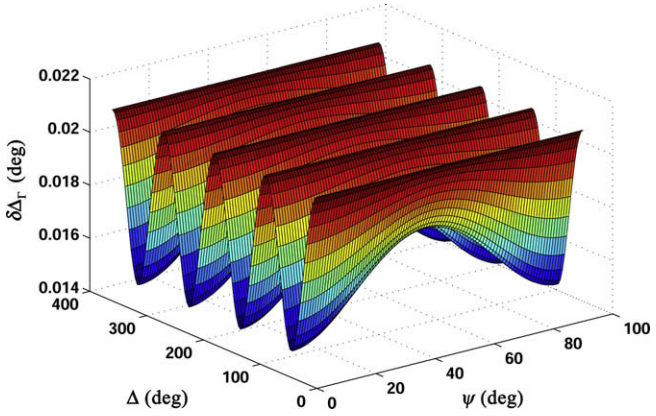

Fig. 2. The uncertainty of Δ induced by phase retardation error of BSC.

where $\delta\Theta_A$ is the misaligned angle. By substituting Eqs. (7c), (9), and (13) into Eqs. (22a) and (22b), the calculated results are

$$(\delta\psi_A)^2 = \cos^2\Delta\left(1 - \frac{1}{2}\sin^2 2\psi\right)(\delta\Theta_A)^2, \tag{23a}$$

$$(\delta\Delta_A)^2 = (2\cot^2 2\psi + \cos^2 2\psi \sin^2 2\Delta)(\delta\Theta_A)^2. \tag{23b}$$

Eq. (23b) is identical to Eq. (19b) of the uncertainty of Δ induced by the misalignment of the polarizer.

Finally, the total uncertainty of ψ and Δ are calculated by using Eqs. (19), (21), and (23). To assume $\delta\Theta_P = \delta\Theta_A = \delta\Theta = 0.1^\circ$ and $\delta\Gamma = 0.03^\circ$, the estimated uncertainties $\delta\psi_t$ and $\delta\Delta_t$ are

$$\delta\psi_t = \left[\left(\frac{1}{2}\sin^2 2\psi \sin^2\Delta + \cos^2\Delta\right)(\delta\Theta)^2\right]^{1/2}, \tag{24a}$$

$$\delta\Delta_t = \left[(4\cot^2 2\psi + 2\cos^2 2\psi \sin^2 2\Delta)(\delta\Theta)^2 + \frac{1}{2}\left(\sin^4\Delta + \cos^4\Delta + \frac{1}{4}\sin^2 2\psi \sin^2 2\Delta\right)(\delta\Gamma)^2\right]^{1/2}. \tag{24b}$$

It is clearly seen that $\delta\psi_t$ is independent of $\delta\Gamma$, while $\delta\Delta_t$ is simultaneously dependent upon $\delta\Theta$ and $\delta\Gamma$. From Eq. (24a), $\delta\psi_t$ varies in a small range in full range of Δ and ψ as shown in Fig. 3. According to Eq. (24b), there is no significant uncertainty on $\delta\Delta_t$ in the full range of Δ ($0^\circ < \Delta < 360^\circ$). However, when ψ is close to 0° or 90°, $\delta\Delta_t$ becomes large because of the first term in Eq. (24b) (see Fig. 4). This is similar to the results obtained in RAE and RCE induced by optical misalignment [23,24]. Theoretically, these results show the advantages of DPPSE on detected uncertainties of Δ and ψ over conventional RAE or RCE of photometric ellipsometer.

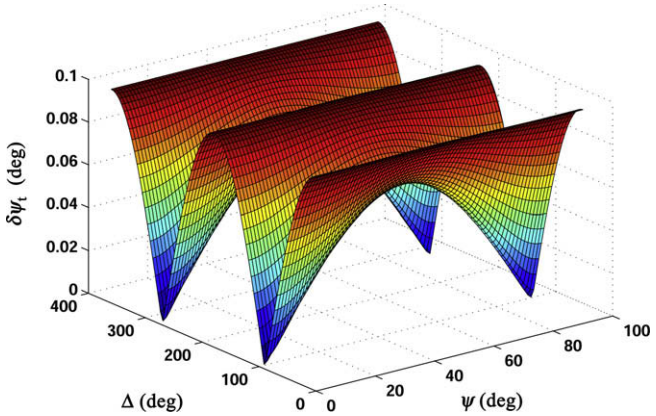

Fig. 3. The uncertainty of ψ results from all error sources.

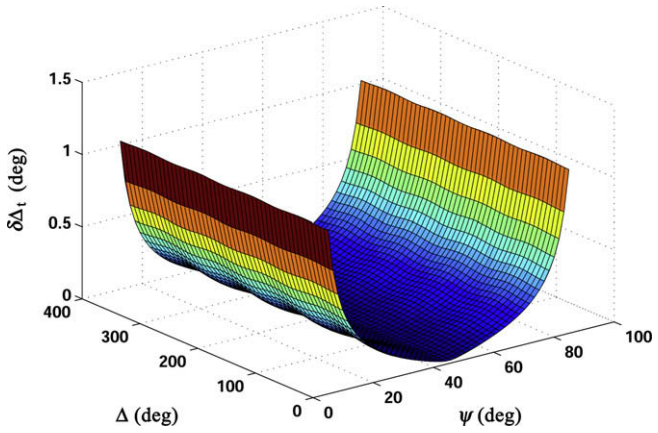

Fig. 4. The uncertainty of Δ results from all error sources.

5. Conclusions

A novel dual-frequency paired polarization phase shifting ellipsometer is developed and the capability of accurate EP measurement is experimentally demonstrated. A dual-frequency paired linear polarizations which are highly correlated, equal amplitude and zero phase difference is integrated into the common-path DPPSE. The working principle is described and the experimental verification is demonstrated in this study. Moreover, the error analysis on EP measurements caused by misalignment of the polarizer and analyzer, or the error of phase retardation of BSC are likewise derived and discussed. To summarize, the features of DPPSE are: (a) dual-frequency equal amplitude and zero phase difference of paired linearly polarized laser beam, (b) common-path phase shifting heterodyne interferometer, (c) amplitude-sensitive detection, (d) full dynamic range of $0^\circ < \psi < 90^\circ$ and $0^\circ < \Delta < 360^\circ$, (e) insensitivity to laser intensity fluctuation, and (f) high sensitivity in EP measurement. In addition, the scattering and absorption of the specimen are likewise insensitive to DPPSE owing to the properties of dual-frequency linearly polarized laser beam and heterodyne detection [17]. Experimentally, Δ can be accurately determined by DPPSE near $\Delta \simeq 0^\circ$ or 180° for low absorbed materials. This is in contrast to the conventional RAE where the uncertainty of Δ becomes large when Δ is close to 0° or 180°. In the experiment, a bare silicon wafer was tested and the ability of DPPSE is verified successfully. Finally, the common-path noise rejection mode is also available in DPPSE. This results in insensitivity to environmental disturbance. According to error analysis, the phase retardation error of BSC affects Δ only and not on ψ determination. Theoretically, however, the misalignment of polarizer or analyzer does affect both ψ and Δ simultaneously in this phase shifting ellipsometer.

Acknowledgments

This research was partially supported by National Science Council of Taiwan through Grant # NSC 96-2221-E-010-002-MY2. The support from the program of "Aim for the top University Plan" is also appreciated.

References

[1] R.M.A. Azzam, N.M. Bashara, Ellipsometry and Polarized Light, North-Holland, Amsterdam, 1987 (Chapter 3).
[2] K. Riedling, Ellipsometry for Industrial Applications, Springer-Verlag, New York, 1988.
[3] T.E. Jenkins, J. Phys. D: Appl. Phys. 32 (9) (1999) R45.
[4] R. Greef, Rev. Sci. Instrum. 41 (4) (1970) 532.
[5] R.W. Collins, Rev. Sci. Instrum. 61 (8) (1990) 2029.
[6] D.E. Aspnes, J. Opt. Soc. Am. 64 (5) (1974) 639.
[7] D.E. Aspnes, Opt. Commun. 8 (3) (1973) 222.
[8] S.N. Jasperson, S.E. Schnatterly, Rev. Sci. Instrum. 40 (6) (1969) 761.
[9] S.N. Jasperson, D.K. Burge, R.C. O'Handley, Surf. Sci. 37 (1973) 548.
[10] F.A. Modine, G.E. Jellison Jr., G.R. Gruzalski, J. Opt. Soc. Am. 73 (7) (1983) 892.
[11] R.C. O'Handley, J. Opt. Soc. Am. 63 (5) (1973) 523.
[12] D.E. Aspnes, P.S. Hauge, J. Opt. Soc. Am. 66 (9) (1976) 949.
[13] C. Chou, H.K. Teng, C.J. Yu, H.S. Huang, Opt. Commun. 273 (1) (2007) 74.
[14] C.Y. Han, Y.F. Chiao, Rev. Sci. Instrum. 77 (2) (2006) 023107.
[15] C.H. Lin, C. Chou, K.S. Chang, Appl. Opt. 29 (34) (1990) 5159.
[16] C.C. Tsai, C. Chou, C.Y. Han, C.H. Hsieh, K.Y. Liao, Y.F. Chao, Appl. Opt. 44 (35) (2005) 7509.
[17] C. Chou, H.K. Teng, C.C. Tsai, L.P. Yu, J. Opt. Soc. Am. A 23 (11) (2006) 2871.
[18] S.M.F. Nee, C.J. Yu, J.S. Wu, H.S. Huang, C.E. Lin, C. Chou, Opt. Express 16 (6) (2008) 4286.
[19] D.C. Su, M.H. Chiu, C.D. Chen, Precis. Eng. 18 (2) (1996) 161.
[20] Thorlabs, Inc, Soleil-Babinet Compensator Operations Manual, <http://www.thorlabs.com/Thorcat/6500/6570-D01.pdf>.
[21] Step wafer ID 0153 from Mikropack GmbH, Germany. The calibration data sheet of step wafer SiO_2 on Si serial number ID0153, by Dipl-Ing (FH) Michael Kaiser, Labor für Mikrosystemtechnik FH-München, Germany.
[22] P.R. Berington, D.K. Robinson, Data Reduction and Error Analysis for the Physical Sciences, McGraw-Hill, New York, 1992 (Chapter 3).
[23] J.M.M. de Nijs, A. van Silfhout, J. Opt. Soc. Am. A 5 (6) (1988) 773.
[24] R. Kleim, L. Kuntzler, A. El Ghemmaz, J. Opt. Soc. Am. A 11 (9) (1994) 2550.